Electronic Supplementary Material (ESI) for Journal of Materials Chemistry A.

Supplementary Information:

Thiophene-Modified Perylenediimide as Hole Transporting Material in Hybrid Lead Bromide Perovskite Solar Cells

Jaykrushna Das,[a†] Raja Bhaskar Kanth Siram,[b†] David Cahen,[a] Boris Rybtchinski,*[b] Gary Hodes*[a]

[a]Department of Materials and Interfaces, Weizmann Institute of Science, Rehovot 7610001, Israel

[b]Department of Organic Chemistry, Weizmann Institute of Science, Rehovot 7610001, Israel

Full experimental details:

1. Preparation of dense TiO_2 (d-TiO_2) layer:

Fluorine-doped tin oxide (FTO) transparent conducting substrate (Xinyan Technology Ltd., TCO-XY15, 15 Ω/sq) was cleaned sequentially in warm aqueous alconox solution, deionized water, acetone (99%) and ethanol (99.9%) each by sonication for 20 min and followed by drying in a nitrogen stream. A dense TiO_2 (d-TiO_2) blocking layer of *ca.* 100 nm thick was deposited on cleaned FTO substrate by spray pyrolysis of 75 wt.% titanium diisopropoxide bis(acetylacetonate) solution (Aldrich) in isopropanol using air as the carrier gas at around 300-350 ˚C. After cooling, the substrate was annealed in a furnace by two-step annealing process: first at 160 ˚C at a rate of 10 ˚C/min and kept for 1 hour and then increased to 450 ˚C with the same ramp rate and kept for another 1 h at this temperature.

2. Preparation of mesoporous TiO_2 (mp-TiO_2) layer:

The mesoporous titania (mp-TiO_2) layer was prepared by spin coating P25 (donated by Evonik) slurry. The slurry was obtained by grinding 2.0 g P25 and 0.340 mL acetic acid (99%) in a mortar for 5 min. Then, 0.850 mL of deionized H_2O was added drop by drop with continued grinding. It was followed by the addition of 5.0 mL 99% ethanol (EtOH) in small aliquots and mixed by grinding in the same mortar and finally the paste was recovered with another 16.5 mL EtOH, followed by the addition of 8.33 g of a solution made up of 0.1 g of 10 cP ethyl cellulose, 0.1 g of 46 cP ethyl cellulose, 3.33 g α-terpineol and 4.8 g EtOH. The final paste was mixed through ultrasonic homogenization using a probe sonicator (BRANSON Sonifier 150). The above processed mp-TiO_2 paste was spin-coated onto the d-TiO_2 substrate in two steps; the first for 5 s at 500 rpm and the second for 40 s at 4000 rpm. The film was sintered under the same annealing condition as those described above for the dense TiO_2. It was then subjected to treatment with an aqueous solution of 40 mM $TiCl_4$ at 70 ˚C for 30 min followed by the same annealing process mentioned earlier. The thickness of the mp-TiO_2 film was ~ 500 nm.

3. Preparation of mesoporous alumina (mp-Al_2O_3) layer:

The mesoporous alumina (mp-Al_2O_3) layer was prepared by mixing an Al_2O_3 slurry (20 wt% solution in iso-propanol, < 50 nm particle size, Sigma-Aldrich) with the same ethyl-cellulose based described above for TiO_2. The deposition and the annealing conditions were the same as for mp-TiO_2.

4. Synthesis and deposition of $MAPbBr_3$ perovskite/device fabrication:

CH_3NH_3Br (MABr) was prepared by adding 5.0 mL hydrobromic acid (HBr, 48 wt% in water, Sigma-Aldrich) to 5.4 mL of methylamine (MA, 40% in methanol, TCI) in a 100 mL round-bottom flask in an ice-bath for 2 h with stirring. The precipitate was then recovered by removing the solvent in a rotary evaporator at 50 ˚C, rinsing with diethyl ether (99.5%) by stirring the solution for 30 min and filtering. This purification process was repeated three times. After the final filtration, the white solid was collected and dried in a vacuum oven at 60 ˚C for 24 h.

A 40 wt% solution of $MAPbBr_3$ was prepared by mixing 3:1 molar ratio of MABr and $PbCl_2$ (98% Sigma-Aldrich) in anhydrous dimethyl formamide (DMF)(99.8%). The solution was then filtered through a 0.45 μm PTFE filter and subsequently spin-coated on the substrate in two steps: 5 s at 500 rpm and then 6000 rpm for 40 s. The substrate was then heated at 150 ˚C on a hot plate for 50 min. The spin coating and the annealing processes were carried out in a chamber under 20-30% humidity. Subsequently, 20 mg of the synthesized hole transporting material (Th-PDI) was dissolved in 1 mL chlorobenzene (99%) and deposited by spin-coating at 500 rpm for 5 s and then 1500 rpm for 45 s. The HTM was doped by mixing the 1 mL of solution with 3.8 μL lithium-bis(trifluoromethanesulfonyl)imide (Li-TFSI, 170 mg dissolved in 1 mL acetonitrile) and 1.8 μL 4-tertbutylpyridine (4-tBP) (96%). Spiro-OMeTAD and CBP were deposited as described in the literature.[1,2] The samples were left overnight in the dark in dry air. Finally, a 80-100 nm thick gold contact was deposited by thermal evaporation (99.999% gold) on the back through a shadow rectangular mask of area 0.24 cm^2.

5. Synthesis of N,N'-bis(ethylpropyl)-1,7-bis(5-*n*-hexyl-2-thienyl)perylene-3,4,9,10-diimide (Th-PDI) :

All solvents were analytical grade. 2-*n*-hexyl thiophene (97%) and tributyl tin chloride (96%) were as-received from Sigma-Aldrich. 2-*n*-hexyl-5-tributylstanylthiophene and 1,7-dibromo perylene-3,4,9,10-diimide (**DBr-PDI**) were synthesized according to literature procedures.[3,4] **DBr-PDI** was recrystallized twice from a dichloromethane (99.5%):hexane (95%) (1:1 v/v) mixture and the purity of 1,7 isomer (>96%; 1,6 isomer <4%) confirmed by NMR spectroscopy

DBr-PDI (0.7g, 1eq) and 2-*n*-hexyl-5-tributylstanyl thiophene (1.163 g, 2.5 eq) were dissolved in 20 mL of toluene (99.5%) under argon atmosphere. Tetrakis triphenylphosphine palladium (0) (99% 0.071 g, 0.06 eq) was added to the reaction mixture and purged with nitrogen for about 15 min. The reaction mixture was heated to 100 ºC for about 8 h under nitrogen atmosphere. Progress of the reaction was monitored by thin layer chromatography (TLC). After completion of the reaction, the mixture was cooled to room temperature and 50 mL distilled water added. The reaction mixture was extracted with dichloromethane and the organic layer washed with saturated aqueous NaCl solution. The dichloromethane layer was dried over anhydrous $MgSO_4$ and concentrated by rotary evaporation till all the solvents were evaporated. The product was purified by column chromatography using dichloromethane as elutant.

Yield: 0.72 g, (82.1 %)

Material characterization

NMR . ^{1}H NMR and ^{13}C NMR spectra were recorded using a Bruker 300 MHz spectrophotometer. Chemical shifts shown below are given in parts per million (ppm) and coupling constants (J) in Hertz.

^{1}H NMR (300 MHz, $CDCl_3$): δ 8.65 (S, 2H), 8.22 (d, J = 1.8Hz, 4H), 7.13 (d, J = 3.6Hz, 2H), 6.83 (d, J = 3.6Hz, 2H), 5.09-4.99 (m, 2H), 2.87 (t, J = 7.5Hz, 4H), 2.30-2.19 (m, 4H), 1.95-1.86 (m, 4H), 1.73-1.66 (m, 4H), 1.38-1.25 (m, 12H), 0.90 (t, J = 7.2Hz, 18H).

^{13}C NMR (75 MHz, $CDCl_3$): δ 149.5, 141.0, 133.6, 133.0, 129.4, 129.2, 128.0, 127.2, 125.7, 57.5, 31.5, 30.3, 28.7, 25.0, 22.6, 14.1, 11.3.

HRMS (m/z): calculated for $C_{54}H_{58}N_2O_4S_2$ 862.3838; found 885.3727 [M+Na]+.

Absorption and photoluminescence spectra were characterized using a Varian Cary 5000 UV-Vis-NIR Spectrophotometer and Varian Cary Eclipse Fluorimeter, respectively. Spectroscopic measurements were performed in standard quartz cells (1 cm x 1 cm). All measurements were carried out at room temperature.

Electrochemical measurements were performed with a CH Instruments electrochemical workstation, model 660C with a platinum disc as working electrode substrate, Ag/AgCl as reference electrode and platinum wire as counter electrode, in dry dichloromethane at a scan rate of 100 mV/s.

Ultraviolet Photoelectron Spectroscopy (UPS) Measurement:

UPS measurements were carried out using a Kratos AXIS ULTRA system, with a concentric hemispherical analyzer for photoexcited electron detection. UPS was measured with a helium discharge lamp, using He I (21.22 eV) and He II (40.8 eV) radiation lines. The total energy resolution was better than 100 meV, as determined from the Fermi edge of an Au reference sample. Al UPS spectra were measured with a -5 V bias applied to the sample to observe photoemission onset at low kinetic energies.

Kelvin Probe Measurement for determination of Work Function:

Contact potential difference (CPD) measurements were performed in a custom-built Kelvin probe system with a Besocke Delta-Phi controller and gold mesh probe. All measurements were performed in a nitrogen-filled glovebox. Samples were placed in the glovebox and were allowed to stabilize until the drift was reduced to less than 1 mV/min. In order to estimate work functions for each sample, the CPD of a freshly-peeled surface of highly oriented pyrolytic graphite (HOPG) was measured as a reference of known work function. The polarity of the Kelvin probe system was check by CPD measurement of gold and aluminum films. The work function of the sample was estimated from the CPD of HOPG and the CPD of the sample as $WF_{sample} = WF_{HOPG} + (CPD_{sample} - CPD_{HOPG})$.

6. Device Characterization:

The current-voltage curves of the devices were measured with a Keithley 2400-LV SourceMeter and controlled with a Labview-based, in-house written program. A home-built solar simulator equipped with a xenon arc lamp and AM1.5 filter whose power output was adjusted to match AM 1.5 global sunlight (100 mW/cm^2) by using a reference Si photodiode (IXOLAR^{TM} High Efficiency SolarBIT, IXYS KXOB22-12X1L) as well as calibrating against natural sunlight measured by an Eppley pyranometer was used for illumination. The device was characterized through a 0.16 cm^2 mask and at a scan rate of 120 mV/s in both forward (Jsc → Voc) and reverse (Voc → Jsc) direction.

The EQE was measured with a Thermo Oriel monochromator with the light chopped at 10 Hz. The current was measured using an Oriel Merlin and TTI PDA-700 photodiode amplifier. The EQE was calculated by referencing to the spectral response of a Si photodiode with a known EQE.

Both plan view and cross-sectional images were taken using a Leo Ultra 55 scanning electron microscope (SEM) with 2-5 kV accelerating voltage.

7. References:

1. Y. Tidhar, E. Edri, H. Weissman, D. Zohar, G. Hodes, D. Cahen, B. Rybtchinski and S. Kirmayer, *J. Am. Chem. Soc.*, 2014, **136**, 13249-13256.
2. P. Docampo, J. M. Ball, M. Darwich, G. E. Eperon and H. J. Snaith, *Nat. Commun.*, 2013, **4**, 2761.
3. J. L. Brusso, O. D. Hirst, A. Dadvand, S. Ganesan, F. Cicoira, C. M. Robertson, R. T. Oakley, F. Rosei and D. F. Perepichka, *Chem. Mater.*, 2008, **20**, 2484-2494.
4. P. Rajasingh, R. Cohen, E. Shirman, L. J. W. Shimon and B. Rybtchinski, *J. Org. Chem.*, 2007, **72**, 5973-5979.

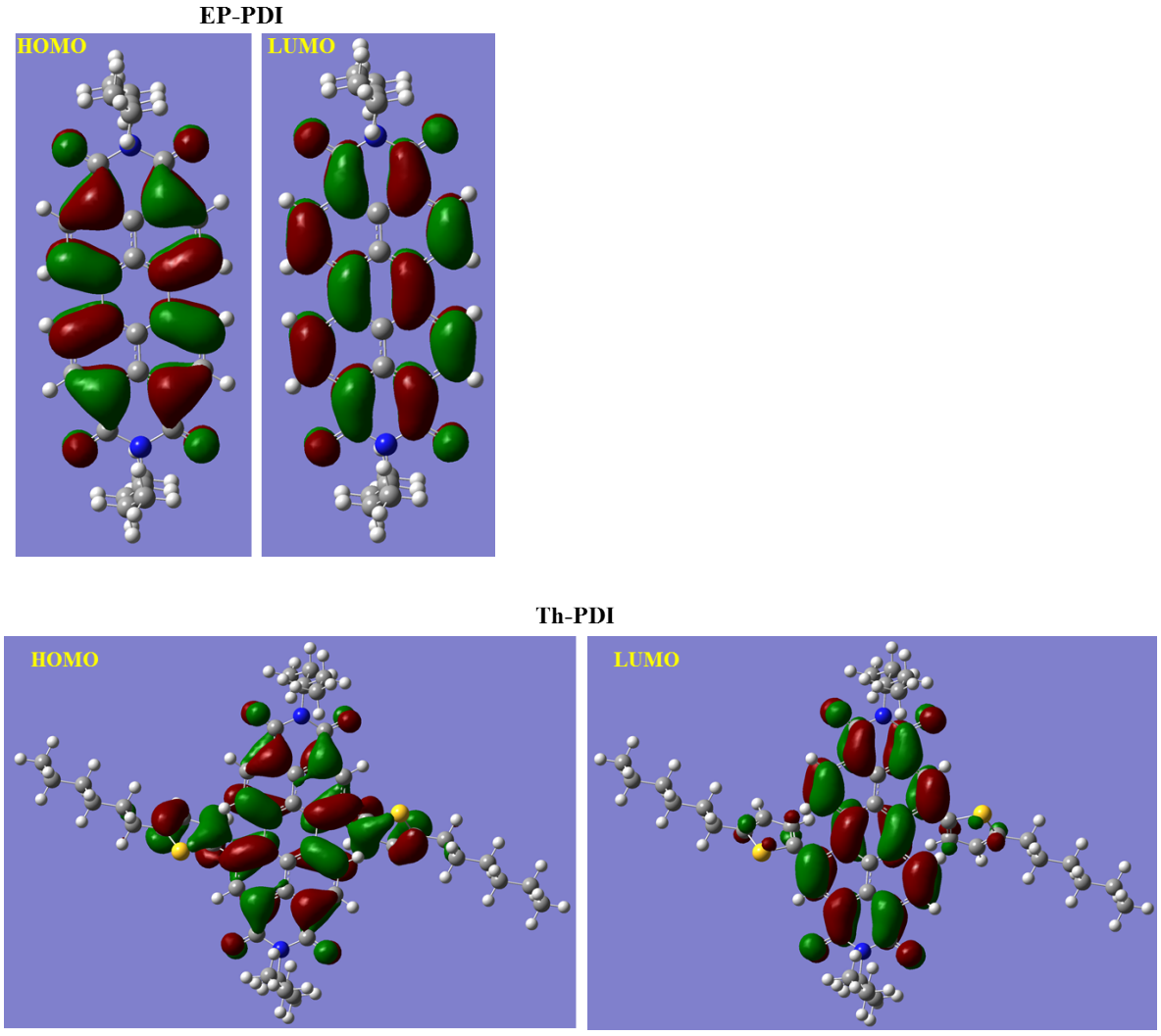

Figure S1: Electron density distribution of HOMO and LUMO a)EP-PDI and b) Th-PDI (grey – carbon; white – hydrogen; blue – nitrogen; yellow - sulphur).

DFT calculations: The ground-state geometry of Th-PDI and its parent compound EP-DPI are fully optimized using density functional theory (DFT) based on the B3LYP/6-31G method as implemented in Gaussian 03 (Fig. S1) in the gas phase. In EP-PDI, the electron density is localized on the perylenediimide core in both the HOMO and LUMO. In case of Th-PDI, the electron density is distributed on both thiophene and the perylenediimide core in the HOMO level, while the electron density of the LUMO is mainly localized on the perylenediimide core only. This indicates the good intramolecular charge-transfer behavior of Th-PDI.

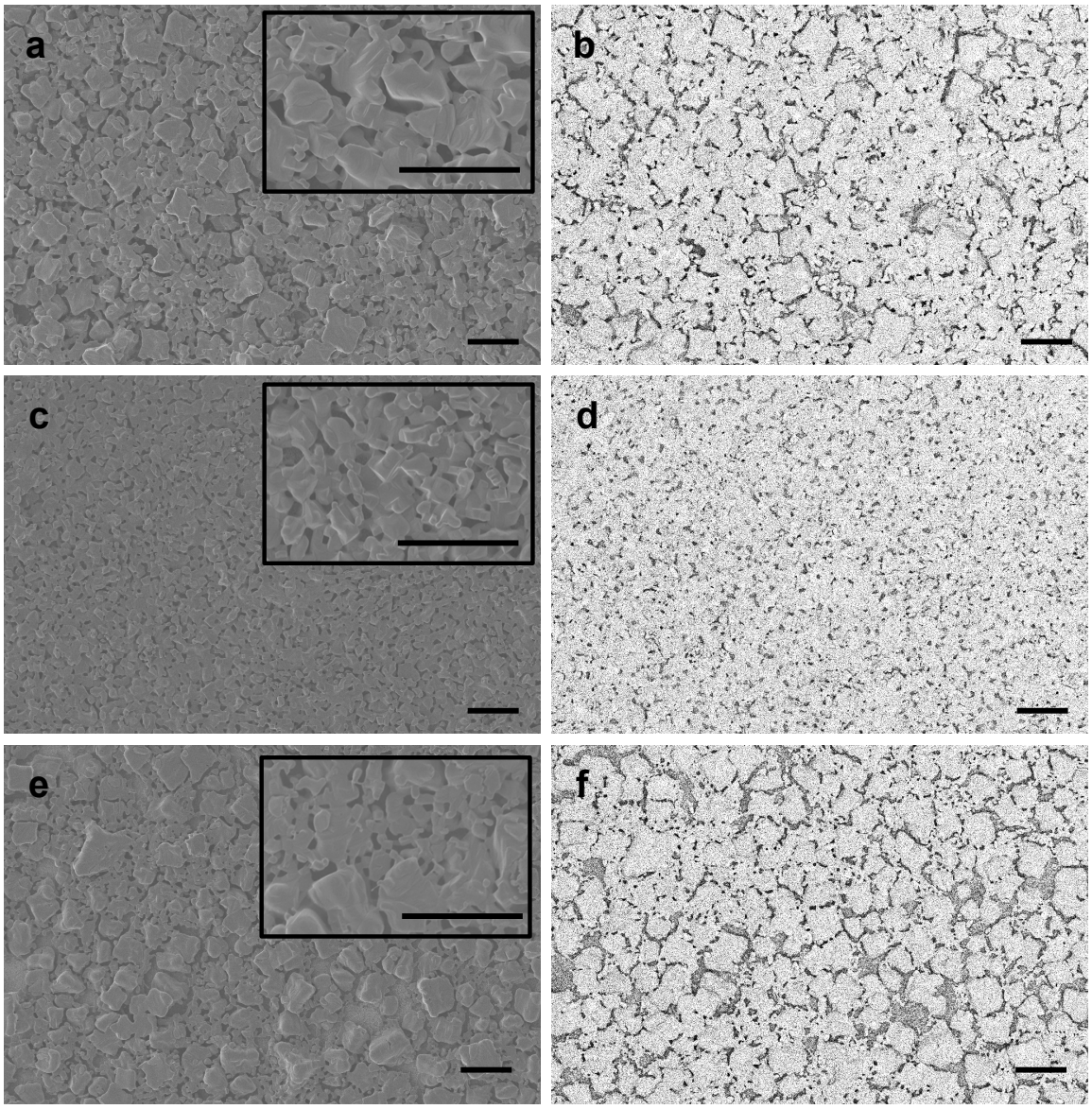

Figure S2. SEM plan views of $CH_3NH_3PbBr_3$ films showing the effect of the different substrates on perovskite coverage deposited by spin-coating; a-b) FTO/d-TiO_2, c-d) FTO/d-TiO_2/mp-TiO_2 and e-f) FTO/d-TiO_2/mp-Al_2O_3. Left hand side: Secondary electron imaging and Right hand side: Backscattered electron detection of the corresponding images shown in the top row. Inset: Higher magnification images. Scale bars in all cases are 5 μm.

Morphological analyses of the film was done by scanning electron microscopy (SEM) to reveal any effect of film morphology and/or surface coverage on the photovoltaic performance of the three different cell types used in this work. Plan views of $CH_3NH_3PbBr_3$ films on various substrates are shown in Figure S1. For the planar and the alumina substrates, the morphologies are very similar with grains of a few μm together with smaller sub-μm grains and moderate coverage (a and e in Fig. S1). For the mp-TiO_2 substrates, the grain size is several times smaller and the coverage better (b in Fig. S1). The backscattered electron images more clearly show the coverage of the different samples. The brighter regions originate from the Pb in the perovskite while the darker regions originate from Ti or Al of the exposed TiO_2 or Al_2O_3. The better coverage of the film on mp-TiO_2 substrate could partially explain why the device made on mp-TiO_2 generates more photocurrent and higher efficiency (Table 2 in the main article).

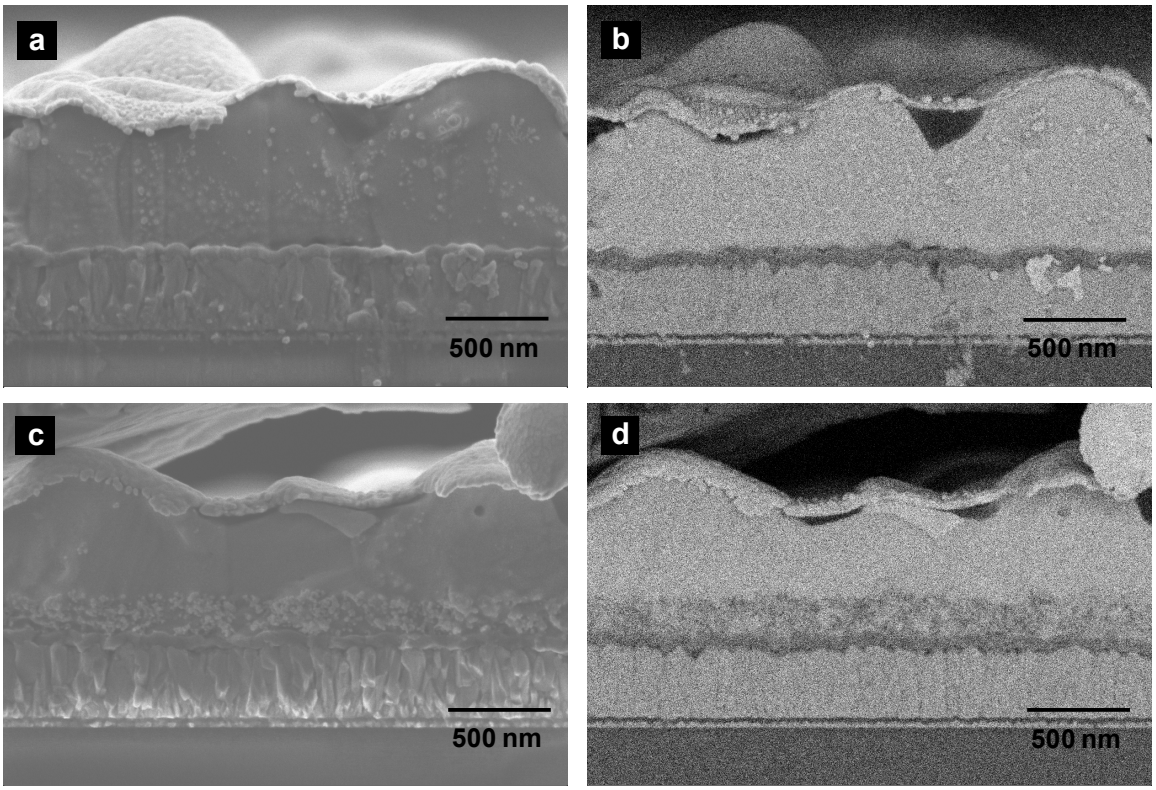

Figure S3. Cross-sectional SEM image of a full-device on (a,b) d-TiO_2 and (c,d) mp-Al_2O_3 substrate. Left side: Images with secondary electron detectors and Right side: Images with backscattered electron detectors.

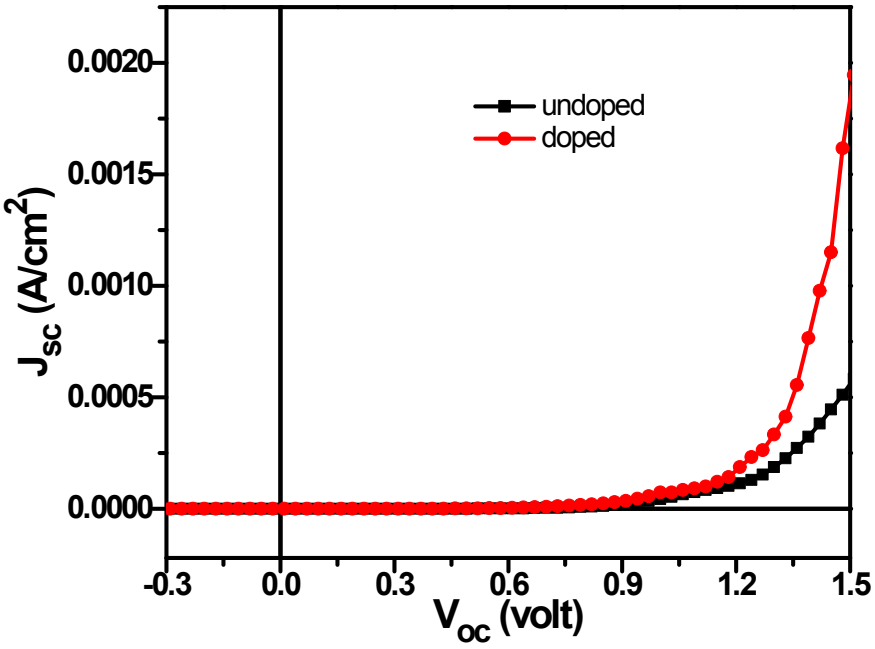

Figure S4. Dark *J-V* curve of a $CH_3NH_3PbBr_3$ cell on mp-TiO_2 substrate with both undoped and doped of HTM. Cell structure: FTO/d-TiO_2/mp-TiO_2/perovskite/Th-PDI/Au. The undoped sample shows a higher series resistance.

Table T1. Photovoltaic parameters of devices prepared in different batches showing the reproducibility of cell structure FTO/d-TiO_2/mp-TiO_2/perovskite/Th-PDI/Au.

Batch No.	J_{sc} (mA/cm^2)	V_{oc} (volt)	FF (%)	η (%)
batch 1	7.3	1.18	61.1	5.3
	7.0	1.21	59.7	5.1
	6.8	1.21	57.6	4.7
	6.6	1.21	60.8	4.9
	6.6	1.21	61.1	4.9
	7.0	1.21	56.3	4.8
batch 2	7.6	1.23	60.7	5.6
	7.2	1.21	59.5	5.2
	6.9	1.21	58.4	4.9
	6.8	1.21	55.1	4.5
	7.0	1.21	56.9	4.8
	6.8	1.21	55.4	4.6
batch 3	7.1	1.21	58.9	5.0
	7.0	1.21	56.7	4.8
	6.8	1.21	58.4	4.8
	7.0	1.21	58.4	5.0
	6.9	1.21	58.9	4.9
	6.8	1.21	59.1	4.9
batch 4	7.6	1.21	56.3	5.2
	7.3	1.21	54.8	4.8
	7.4	1.18	60.4	5.3
	6.7	1.21	59.5	4.9
	6.7	1.21	60.1	4.9
	6.9	1.21	57.8	4.8

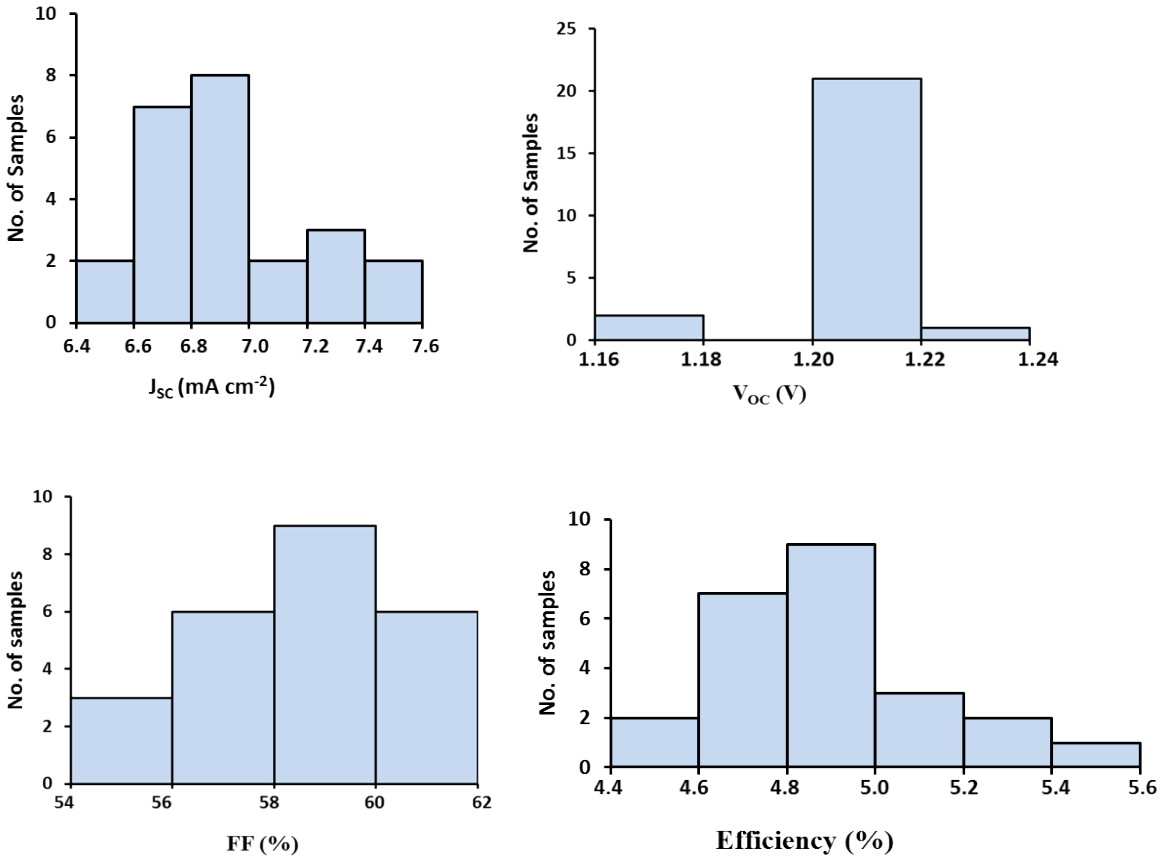

Figure S5. Data from Table T1 in histogram form with all batches taken together.

Table T2. Photovoltaic parameters of devices prepared in different batches on mp-Al_2O_3.

Batch No.	**J_{sc} (mA/cm^2)**	**V_{oc} (volt)**	**FF (%)**	**η (%)**
batch 1	2.7	1.41	52.9	2.0
	2.3	1.39	53.6	1.7
	2.4	1.39	52.8	1.8
	2.4	1.39	58.9	1.9
	2.7	1.41	56.2	2.2
batch 2	2.8	1.39	47.2	1.8
	2.3	1.36	60.3	1.9
	2.7	1.41	52.9	2.0
	2.5	1.36	51.6	1.7
	2.8	1.39	53.6	2.1
batch 3	2.5	1.36	51.0	1.8
	2.5	1.36	51.6	1.7
	2.6	1.35	60.8	2.1
	2.8	1.41	47.3	1.9
	2.4	1.41	55.9	1.9

Table T3. Photovoltaic parameters of devices prepared in different batches on d-TiO_2.

Batch No.	J_{sc} (mA/cm^2)	V_{oc} (volt)	FF (%)	η (%)
batch 1	3.0	1.27	42.4	1.6
	3.4	1.24	57.2	2.4
	3.3	1.24	56.1	1.3
	2.9	1.27	56.0	2.1
	3.2	1.24	55.7	2.2
batch 2	3.0	1.24	56.2	2.1
	3.1	1.27	47.3	1.9
	3.5	1.27	66.6	2.9
	3.2	1.24	64.7	2.6
batch 3	3.4	1.27	65.9	2.9
	3.1	1.24	56.8	2.2
	3.0	1.27	65.7	2.5
	3.2	1.27	67.1	2.7
	3.0	1.27	68.1	2.6
batch 4	3.4	1.27	64.3	2.8
	2.8	1.24	64.9	2.3
	3.2	1.24	65.9	2.6
	3.2	1.24	67.0	2.7

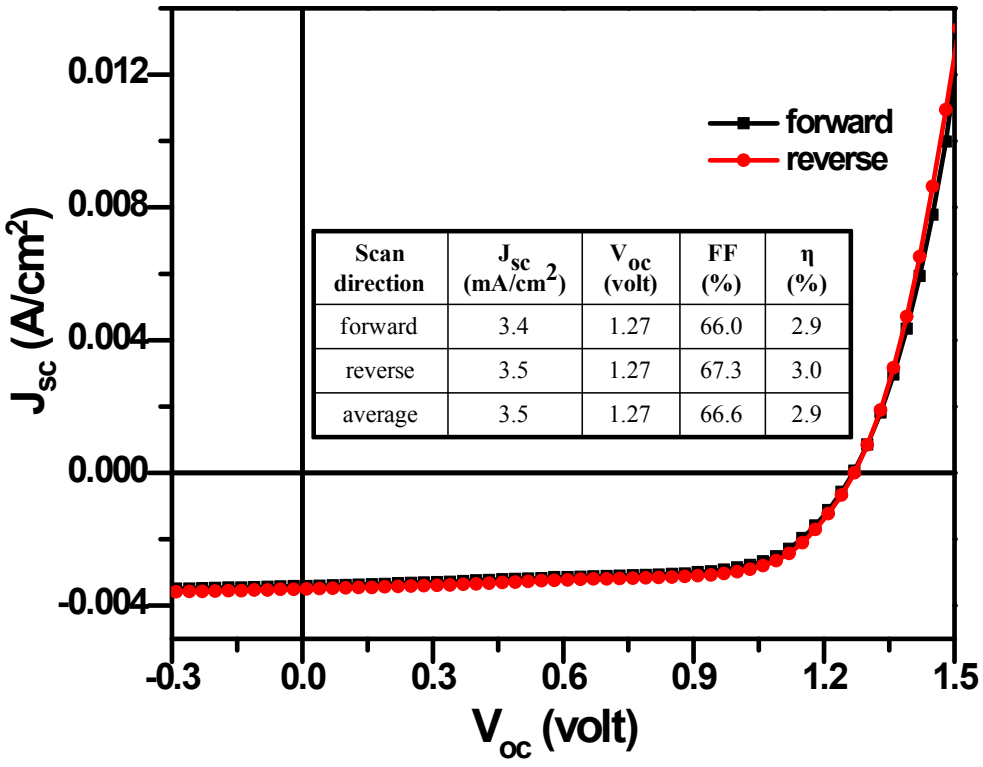

Scan direction	J_{sc} (mA/cm^2)	V_{oc} (volt)	FF (%)	η (%)
forward	3.4	1.27	66.0	2.9
reverse	3.5	1.27	67.3	3.0
average	3.5	1.27	66.6	2.9

Figure S6. Photocurrent density-voltage (*J-V*) curves of a planar cell (FTO/d-TiO_2/perovskite/Th-PDI/Au) measured in both sweep directions. Inset: The photovoltaic-parameters of the cell.

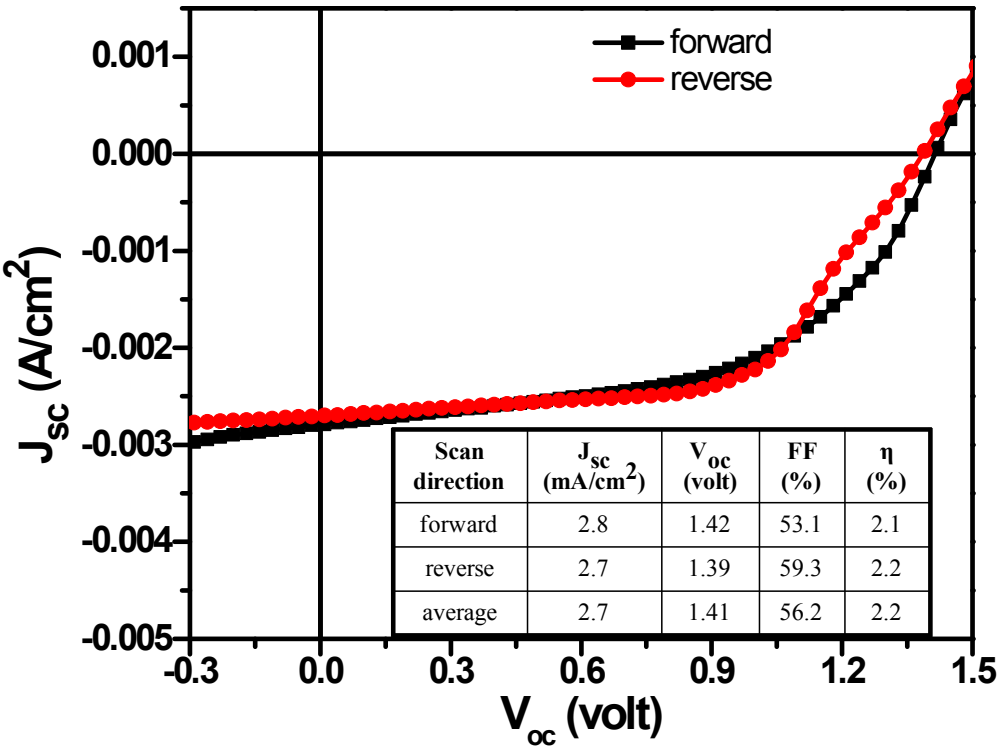

Scan direction	J_{sc} (mA/cm^2)	V_{oc} (volt)	FF (%)	η (%)
forward	2.8	1.42	53.1	2.1
reverse	2.7	1.39	59.3	2.2
average	2.7	1.41	56.2	2.2

Figure S7. Photocurrent density-voltage (*J-V*) curves of a meso-superstructured Al_2O_3 cell (FTO/d-TiO_2/mp-Al_2O_3/perovskite/Th-PDI/Au) measured in both sweep directions. Inset: The photovoltaic-parameters of the cell.

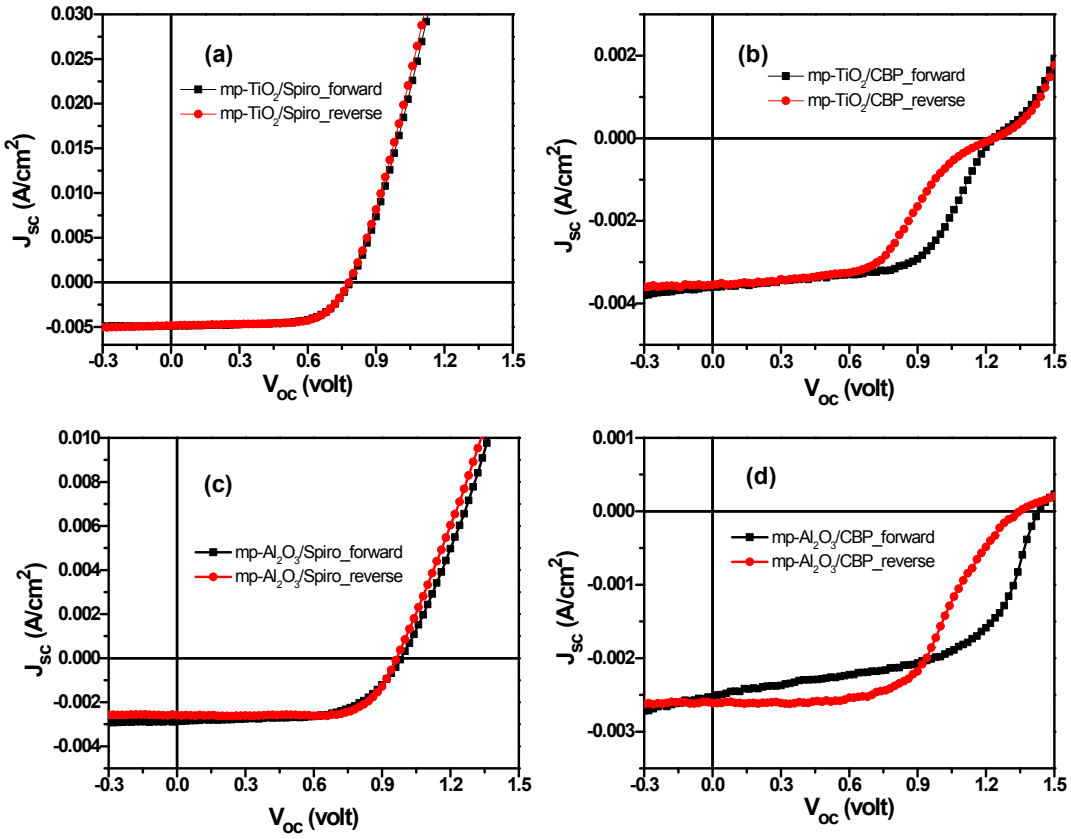

Figure S8. Photocurrent density-voltage (*J-V*) curves of $CH_3NH_3PbBr_3$ cells on mp-TiO_2 (a,b) and mp-Al_2O_3 (c,d) substrates with spiro-OMeTAD (a,c) and CBP (b,d) as HTMs and measured in both sweep directions. The degree of hysteresis is very different for the different HTMs and to some, but lesser extent for the two different mp-oxide substrates.